(Received 1 December 2024, Accepted 24 January 2025, Scheduled 6 February 2025)

The Problem of Determining the Characteristics of Optical Semiconductors in Plasma Antennas Design and Its Solutions

Mikhail S. Shishkin*, Pavel A. Titovets, and Mikhail O. Fedyuk

Science and Research Department, Moscow Technical University of Communication and Informatics, Moscow, Russia

ABSTRACT: The article focuses on the problem of determining optical semiconductor cell characteristics that can be used for plasma antenna development. The problem outlined is associated with the insufficient characteristics (for example, electrical conductivity) in datasheets for semiconductors on the market, which are for the simulation of antennas. An optical semiconductor conductivity calculation method, when representing it as a segment of a microstrip transmission line (a coplanar waveguide) with a known transmission coefficient (S_{21}) as a radio frequency signal passes through it, is suggested. The article presents a simple and easy-to-use experimental setup for the trial of the suggested method. The essence of the method lies in using a PCB with a microstrip line with a gap in the middle. SMA ports for connection with a vector network analyzer are on the edges. A studied optical semiconductor cell is placed at the transmission line gap, and the transmission coefficient between the two ports can be measured. In addition to that, the conductivity of the cell under illumination can be calculated based on the proposed formulas. The article presents the results of measuring some optical semiconductor cells (resistors, diodes, transistors) and their conductivity calculations under illumination. The results obtained on the conductivity of photocells can be used for simulating antennas that involve optical semiconductor cells.

1. INTRODUCTION

As it is known, plasma is understood as a state of dielectric material where conductive properties are to prevail under certain physical stimuli. The most well-known material from the physics theory is a gas, which ionizes under high temperatures, acquiring the property of conductivity [1–4]. In modern antenna engineering, gas plasma is rarely used for several reasons. Firstly, it is connected to the complexity of creating a body of a certain shape from the gas to form an antenna or its certain elements. Secondly, the gas ionization process demands more energy, complicating the antenna design and its following maintenance [4–6].

It has long been known that semiconductors are used in antenna and microwave engineering. PIN diodes are more frequently used as keys in phase shifters [7–10], various microwave switches [11–13], and antennas where, for example, polarization switching or alteration of the operating frequency range is required [14–20]. However, modern antenna engineering knows solutions utilizing PIN diodes in plasma antenna designs [21–26]. In the simplest case, the PIN diode has two states:

- Closed: it has high resistance, and it is treated as a high impedance resistor without bias voltage.
- Opened: the diode operates as a conductor under a bias voltage.

The use of PIN diodes in microwave and antenna engineering poses some challenges, the most fundamental of which is the necessity of a constant control voltage supply to the microwave circuit. Such a circuit would work simultaneously with zero and high-frequency currents, which leads to a few tasks to ensure high isolation between the radio signal input and control voltage input to improve the electromagnetic compatibility (EMC) performance of the device. DC and high-frequency current isolations are not always achievable at the required level; in addition, this process makes the whole design using PIN diodes significantly more complex and often makes microwave characteristics of the circuit worse due to the loss of some power on the filters providing the required electrical isolation.

Applying optical cells, where conductor properties change by light instead of direct voltage, eliminates any electromagnetic interactions of the control circuit and the microwave circuit without additional devices or circuit solutions, enhancing the isolation between circuits. Moreover, there are known results where conductivity characteristics change smoothly under controlled illumination of different power levels that can be used in certain microwave designs or antennas, for example, a phase shifter with a smooth phase shift or an antenna with a smooth tuning operating frequency change. Optical cells (or photocells) are reflected in antenna design and microwave devices with switchable parameters where the photocell works as a key-like design with PIN diodes. Furthermore, research on plasma antennas, involving ionized semiconductors as high-frequency current conductor elements instead of standard metallic conductors, is getting more comprehensive [27–31].

Simulation is a crucial process in the design of any antenna. The more the parameters are considered, the more the simu-

* Corresponding author: Mikhail S. Shishkin (mikkhail666@gmail.com).

lation outcomes match the predicted experimental results. The conductivity values of conductor elements and permittivity values of dielectric ones are vital for 3D simulation. In [4], various methods are given for assessing the characteristics of a gas plasma column for simulating gaseous plasma antennas. There are a number of papers devoted to the study of the characteristics of photosensitive semiconductor cells. The topic of photovoltaic solar cells has been studied the most in this area [32–36], but publications are mainly devoted to modeling, calculation, and measurement of the current-voltage characteristics (photoefficiency) of cells under the influence of light, aimed, among other things, at further improvement of such elements (increasing their efficiency).

There are analytical formulas, such as those mentioned in [31, 37–38], that simplify the determination of the conductivity and permittivity of a photocell with a known chemical composition. Yet, it is almost impossible to analytically determine the electrical characteristics of a semiconductor cell on the market. In this regard, the problem of identifying the conductivity and permittivity of a photocell is a significant and relevant task.

In the article, we present a method for determining photocell conductivity and using it as a segment of a microstrip transmission line (MTL) or a coplanar waveguide (CPW) with known characteristics. The method solves the problem of determining the conductivity of a photocell based on the measured transmission coefficient (S_{21}) values using an elementary experimental setup and a vector network analyzer (VNA).

2. FEATURES OF SOME PHOTOCELLS

Photoresistors, photodiodes, and phototransistors are the most often used photocells in modern circuitry. Here we will consider their typical designs, principles, and features.

2.1. Photodiode

A photodiode is a semiconductor photosensitive cell that generates current or voltage under illumination. The basis for generating current or voltage in photodiodes is a PN junction. An unalloyed I-area can be added to apply photodiodes to attenuators, fast switches, photodetectors, high-voltage equipment, etc. The equivalent circuit of a photodiode and its structure are shown in Figures 1–2, where I_L is the current generated by incident light, V_D the voltage across the diode, I_D the diode current, C_j the junction capacitance, R_S the shunt resistance, I_{sh} the shunt current, R_s the series resistance, V_o the output voltage, and I_o the output current.

Under illumination, electron-hole pairs necessary for current flow are formed in the semiconductor. The number of carriers released in the process depends on the material. Absorption constant, determining irradiation efficiency, depends on light's wavelength and describes the effective depth of penetration of light; this dependence is shown in Figure 3 [38].

2.2. Photoresistor

A photoresistor is a passive semiconductor cell that changes its resistance under illumination independently from the direction of current flow. Unlike photodiodes and phototransistors, photoresistors are less sensitive to light. Their photosensitivity depends on the wavelength of light, which varies in different materials. In circuitry, photoresistors are usually shown as resistors of varying resistance values. The equivalent circuit for a photoresistor is shown in Figure 4, where R_j is junction resistance, and C_j is junction capacitance [39].

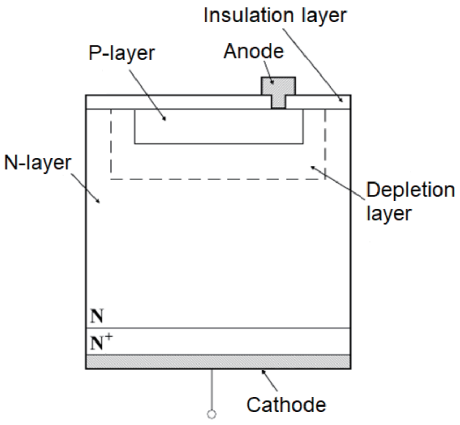

FIGURE 1. Photodiode structure.

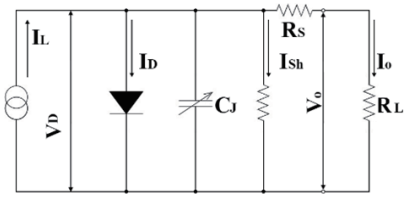

FIGURE 2. Photodiode equivalent circuit example.

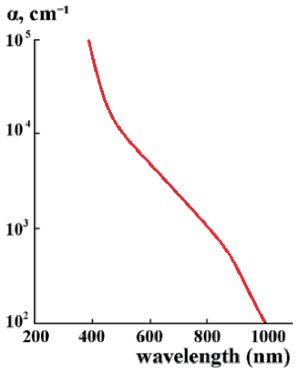

FIGURE 3. Light absorption constant for silicon and germanium at 300 K.

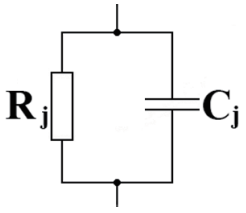

FIGURE 4. Photoresistor equivalent circuit example.

2.3. Phototransistor

A phototransistor is based on photodiodes but has an internal photocurrent amplifier. This increases its photosensitivity, allowing for more efficient operation with lower-power optical radiation sources. Despite their higher sensitivity, phototransistors have a slower response, a higher dark current value, and an internal noise source.

Various types of phototransistors are used to stimulate different equivalent circuits. For example, the article [40] provides the equivalent circuit (Figure 5) for a uni-traveling carrier hetero-junction phototransistor (UTC-HPT), where R_{be} is the base-emitter resistance, C_e the emitter capacitance, V_{be} the base-emitter voltage, C_c the collector capacitance, R_{bc} the base-collector resistance, R_{ce} the collector-emitter resistance, V_{be} the base-emitter voltage, and R_L the load resistance.

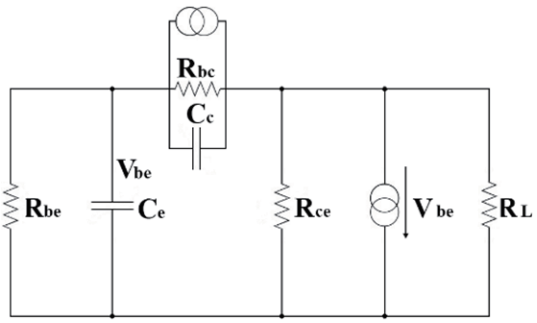

FIGURE 5. UTC-HPT equivalent circuit example.

3. THEORY FOR DETERMINING THE CONDUCTIVITY OF A PHOTOCELL

Let us consider a microstrip transmission line. As known, an MTL consists of a conductor of width w and thickness t, placed on a dielectric substrate with some relative permittivity ε at a height h above the screen (the height in the simplest case corresponds to the thickness of the substrate). For connection of the line to the external sources or receivers, coaxial-to-strip line adapters are usually applied, as shown in Figure 6. The width of the MTL conductor is known to be selected based on the need to provide the required impedance in the line Z, and when the value of $w/h \leq 2$, it can be calculated using the following

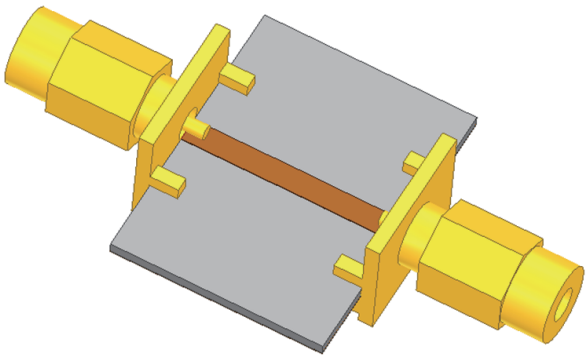

FIGURE 6. The appearance of the microstrip transmission line with microstrip-coaxial transitions.

empirical formula [41–43]:

$$w = \frac{8h}{e^d - 2e^{-d}}, \tag{1}$$

where

$$d = \frac{Z}{60} \cdot \sqrt{\frac{\varepsilon_r + 1}{2}} + \frac{(\varepsilon_r - 1) \cdot \left(0.226 + \frac{0.12}{\varepsilon_r}\right)}{\varepsilon_r + 1}. \tag{2}$$

When $w/h \geq 2$, the width of the MTL conductor can be calculated by the formula [41–43]:

$$w = \frac{2h}{\pi}\left\{\left(\frac{60\pi^2}{Z\sqrt{\varepsilon_r}} - 1\right) - \ln\left(\frac{120\pi^2}{Z\sqrt{\varepsilon_r}} - 1\right) + \frac{\varepsilon_r - 1}{2\varepsilon_r} \times \right.$$
$$\left. \times \left[\ln\left(\frac{60\pi^2}{Z\sqrt{\varepsilon_r}} - 1\right) + 0.39 - \frac{0.61}{\varepsilon_r}\right]\right\}, \tag{3}$$

Line attenuation (dB/m) of electromagnetic waves in an MTL is determined by the sum of losses in the dielectric and metal parts. The attenuation due to dielectric losses can be calculated by the formula [41–43]:

$$\alpha_d = \frac{27.3 \cdot \varepsilon}{\varepsilon - 1} \cdot \frac{\varepsilon_{re} - 1}{\sqrt{\varepsilon_{re}}} \cdot \frac{tg\,(\delta)}{\lambda_0}, \tag{4}$$

where λ_0 is the free space wavelength at the given frequency f, $tg(\delta)$ the substrate loss tangent, and ε_{re} the effective substrate permittivity, determined according to the expression:

$$\varepsilon_{re} = \frac{\varepsilon + 1}{2} + \frac{\varepsilon - 1}{2} \cdot \left(1 + \frac{10 \cdot h}{w}\right)^{-1/2}. \tag{5}$$

The conductor attenuation in an MTL in the simplest case can be calculated by the formula [41–43]:

$$\alpha_c = \frac{8.686 \cdot R_s}{Z \cdot w}, \tag{6}$$

where R_s is the conductor surface resistance:

$$R_s = \sqrt{\frac{\pi \cdot f \cdot \mu_0}{\sigma}}, \tag{7}$$

where μ_0 is the magnetic constant ($\mu_0 = 4\pi \cdot 10^{-7}$), and σ is the MTL conductor conductivity (S/m).

To consider the metal thickness in expressions (1)–(6), we can use the effective width value [41–43]:

$$w_{eff} = \begin{cases} w + 1.25\frac{t}{\pi}\left(1 + \ln\frac{4\pi \cdot w}{t}\right) & \text{for } w \leq 0.5\pi h \\ w + 1.25\frac{t}{\pi}\left(1 + \ln\frac{2h}{t}\right) & \text{for } w \geq 0.5\pi h \end{cases}. \tag{8}$$

In order to increase the isolation, types of transmission lines are used which are quite similar to an MTL — a coplanar

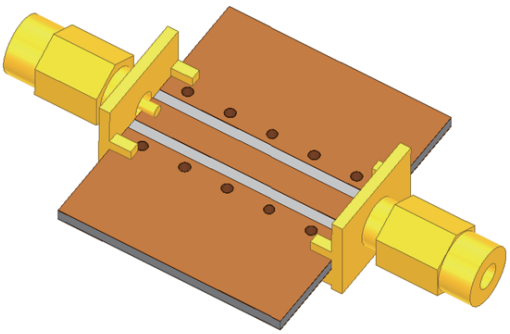

FIGURE 7. The appearance of the grounded coplanar waveguide with coaxial connectors.

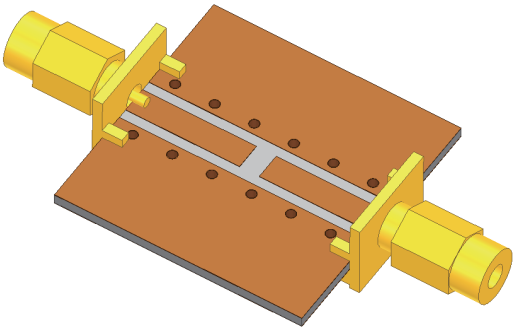

FIGURE 8. The experimental setup appearance for photocell parameters measurements.

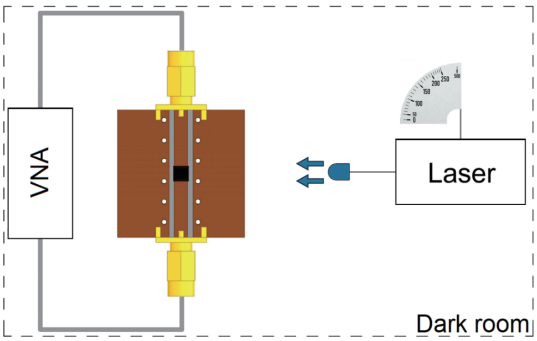

FIGURE 9. The experimental scheme for determination of photocell parameters.

waveguide or its modification — a grounded coplanar waveguide (GCPW). The coplanar waveguide consists of a metal strip with a width w and two adjacent ground planes; the gap between the strip and ground is denoted by S. The grounded coplanar waveguide has a CPW structure that adds vias for mode selection and greater suppression of radiation, i.e., higher isolation (Figure 7).

The effective substrate permittivity of GCPW is determined with the empirical expression [41–43]:

$$\varepsilon_{re} = 1 + \frac{\varepsilon - 1}{2} \cdot \left[\frac{K(k_2)}{K'(k_2)}\right] \cdot \left[\frac{K'(k_1)}{K(k_1)}\right], \tag{9}$$

where $K(k)$ is the complete elliptic integral of the first kind, and the ratio of these functions can be determined as:

$$\frac{K(k)}{K'(k)} = \begin{cases} \dfrac{\pi}{\ln\left(2\frac{1+\sqrt{k'}}{1-\sqrt{k'}}\right)} & \text{for} \quad 0 \le k \le 0.707 \\ \dfrac{1}{\pi} \cdot \ln\left(2\dfrac{1+\sqrt{k}}{1-\sqrt{k}}\right) & \text{for} \quad 0.707 \le k \le 1 \end{cases}, \tag{10}$$

where the arguments for the elliptic integrals k_1 and k_2 can be obtained as:

$$k_1 = \frac{w}{w+2S}, \tag{11}$$

$$k_2 = \frac{\sinh\left[\frac{\pi w}{4h}\right]}{\sinh\left[\frac{\pi(2S+w)}{4h}\right]}. \tag{12}$$

The appearance of the setup for determining photocell parameters is shown in Figure 8. The experimental scheme with VNA is given in Figure 9. The experimental setup is a section of a GCPW shown in Figure 7 (or an MTL shown in Figure 6) with SMA connectors soldered along the edges and a gap in the center, where a photocell is installed. The measuring channels of the VNA are plugged into the connectors, and the complex transmission coefficient is measured. The absolute value of the transmission coefficient $|S_{21}|$ in dB, obtained during measurements, will correspond to the inverse total loss values of the experimental setup:

$$|S_{21}| = -\sum L. \tag{13}$$

According to [41–43], transmission line losses L_{TRL}, except for conductor (or Ohmic) (6) and dielectric losses (4), include radiation losses and mismatch losses. Assuming that the transmission line is matched in the operating frequency range, and its width is significantly less than the resonant size (a quarter of the wavelength) at the operating frequency, the latter can be neglected. The proposed experimental setup includes 3 parts in which losses must be taken into account: connectors at the edges (losses in which L_{SMA} can reach 0.1–0.3 dB), the transmission line itself, and the photocell, losses in which L_{PC} will differ from line losses:

$$\sum L = L_{TRL} + L_{SMA} + L_{PC}. \tag{14}$$

It is obvious that losses in the studied photocell can be obtained from (13) and (14) as follows:

$$L_{PC} = -\left(|S_{21}| + L_{TRL} + L_{SMA}\right). \tag{15}$$

Thus, if we consider the measured photocell as a small piece of transmission line with length l_{PC} equal to its width w_{PC}, based on Equation (7), we can obtain the following approximate formula for determining the conductivity of the measured cell:

$$\sigma_{PC} = \frac{\pi \cdot f \cdot \mu_0}{R_s^2} = \frac{\pi \cdot f \cdot \mu_0}{\left(\frac{\alpha_c \cdot Z_{PC} \cdot w_{PC}}{8.686}\right)^2}$$

$$= \frac{75.45 \cdot \pi \cdot f \cdot \mu_0}{\left(\alpha_c \cdot Z_{PC} \cdot w_{PC}\right)^2} = \frac{75.45 \cdot \pi \cdot f \cdot \mu_0}{\left(\frac{L_{PC}}{l_{PC}} \cdot Z_{PC} \cdot w_{PC}\right)^2}$$

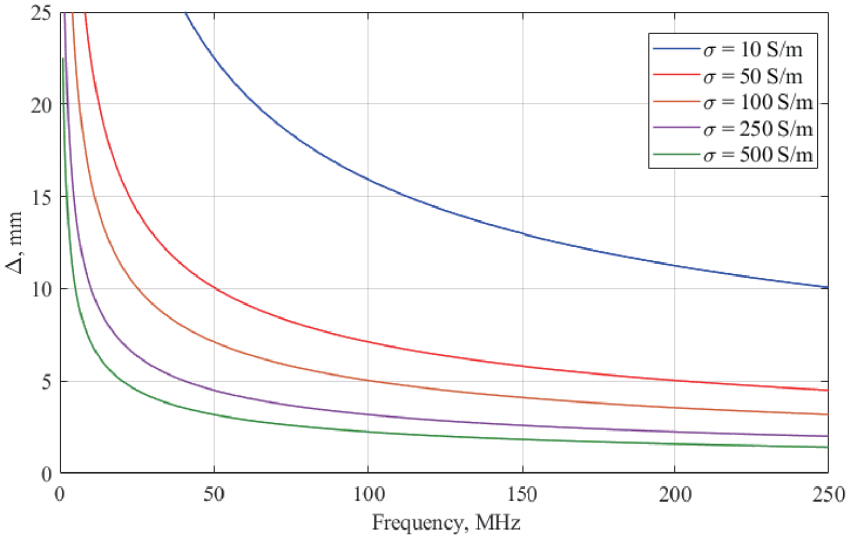

FIGURE 10. The skin depth plots with different conductivity values.

$$= \frac{75.45 \cdot \pi \cdot f \cdot \mu_0}{\left(-|S_{21}| - L_{TRL} - L_{SMA}\right)^2 \cdot Z_{PC}^2}. \quad (16)$$

Since the photocell dimensions are quite small, losses in the conductor are solely considered in expression (16), and the calculation error is expected to be negligible if losses in the dielectric (substrate) are not included.

Phase incursion, when an electromagnetic wave passes through a transmission line of length l_{TRL}, can be determined by the formula:

$$\theta_{TRL} = \frac{2\pi}{\lambda_g} \cdot l_{TRL} = \frac{2\pi \cdot \sqrt{\varepsilon_{re}}}{\lambda_0} \cdot l_{TRL}. \quad (17)$$

Then, the phase incursion, when the wave passes through the transmission line of length l_{TRL} in which the studied photocell of length l_{PC} is installed, will equal:

$$\theta_{PC} = \frac{2\pi \cdot \left\{\left(l_{TRL} - l_{PC}\right)\sqrt{\varepsilon_{re_{SUB}}} + l_{PC}\sqrt{\varepsilon_{re_{PC}}}\right\}}{\lambda_0}. \quad (18)$$

Thus, the effective permittivity of the measured cell will be as follows:

$$\varepsilon_{re_{PC}} = \left\{\frac{\S \cdot \theta_{PC}}{2\pi \cdot f \cdot l_{PC}} - \left(\frac{l_{TRL}}{l_{PC}} - 1\right)\sqrt{\varepsilon_{re_{SUB}}}\right\}^2. \quad (19)$$

If we consider two printed boards, one with a gup for installing a photocell (Figure 8) and the other without it (Figure 7), but their perimeter dimensions are the same, then the phase delay in the photocell will be determined only by the dielectric constant of the cell itself; therefore, the expression (19) can be transformed as follows:

$$\varepsilon_{PC} = \left\{\frac{c \cdot \theta_{PC}}{2\pi \cdot f \cdot l_{PC}} - \frac{l_{TRL}}{l_{PC}}\sqrt{\varepsilon_{re_{SUB}}}\right\}^2. \quad (20)$$

One notes that, in all used equations, we suppose that the used metal parts of the MTL or the GCPW do not have magnetic properties, and, accordingly, the permeability is $\mu \approx 1$.

As known, dielectric losses are the same for both an MTL and a CPW. At first approximation, conductor losses can be considered alone. However, if higher accuracy is necessary, conductor losses can be calculated using a more detailed formula, given, for example, in [43]. Due to its complexity, we will not present it here; we will clarify that at distances S greater than the substrate height h, the error in calculations using formula (16) as applied to GCPW will be no more than 2–3%, which may be sufficient for most problems with simulating the characteristics of a photocell. In this case, formula (20) is valid for both transmission lines under consideration.

As known, when electromagnetic energy propagates along a transmission line, skin effect can be observed as currents flow along the metal surface, and their penetration depth (m) depends on the wave oscillation frequency and the conductor's conductivity:

$$\Delta = \frac{1}{\sqrt{\pi \cdot \mu_0 \cdot \mu_r \cdot f \cdot \sigma}}, \quad (21)$$

where μ_r is the conductor's relative permeability (for non-magnetic metals $\mu_r = 1$).

Understanding the penetration depth of the current is vital for simulation because after reaching a certain conductivity threshold, all calculations are performed only on the surfaces of the elements of the designed antennas or microwave devices. Let us consider the frequency dependences of current penetration depth at different conductivity values of the conductor with $\mu_r = 1$ (Figure 10). From the proposed plots, it is obvious that when metallic elements are calculated, where the conductivity value exceeds 10^7 S/m, at frequencies from a few MHz, the currents are calculated only on the surface of the element. However, when dealing with a semiconductor, the conductivity rarely reaches values of a few hundred S/m and higher, as

shown in [31]. Thus, the calculations should be carried out in their entirety, not only on their surfaces, for simulation.

To simplify, we can certainly use Equation (16), where the calculation is made on the basis of the expression for the surface resistance of the cell; however, for greater accuracy of calculations, the conductivity must be determined for the entire volume of the photocell. Let us analyze formula (6) in more detail. Conduction losses consist of two parts: losses in the stripline and losses in the ground plane:

$$\alpha_c = \alpha_l + \alpha_g = \frac{R_l + R_g}{2Z}, \tag{22}$$

where R_l and R_g are the effective series resistance per unit length of the stripline conductor and ground plane, respectively:

$$R_l = \frac{1}{\Delta_l \cdot \sigma_l \cdot w}, \quad R_g = \frac{1}{\Delta_g \cdot \sigma_g \cdot w}, \tag{23}$$

where Δ_l and Δ_g are the skin depths, and σ_l and σ_g are the conductivities of the stripline and ground plane, respectively.

According to the expressions, we see that the skin effect is taken into account when the conduction losses of the transmission line are calculated. On the one hand, based on the plots in Figure 10 and taking into account the previously proposed conclusions, it can be assumed that in expressions (22) and (23), the skin depths can be taken equal to half the thickness of the photocell $t_{PC}/2$. On the other hand, without being tied to the specific size of a cell and the understanding that its conductivity will always be quite low, we obtain a refined expression for calculating conductor losses (dB/m) in the studied photocell:

$$\alpha_c = 8.686 \cdot \frac{\sqrt{\pi \cdot \mu_0 \cdot f}}{2Z_{PC} \cdot w_{PC}} \cdot \left(\frac{1}{\sqrt{\sigma_g}} + \frac{1}{\sqrt{\sigma_{PC}}} \right). \tag{24}$$

Then, the previously presented expression (16) for calculating the photocell conductivity will take the following form:

$$\sigma_{PC} = \frac{18.86 \cdot \pi \cdot f \cdot \mu_0 \cdot \sigma_g}{\left(-|S_{21}| - L_{TRL} - L_{SMA}\right)^2 \cdot Z_{PC}^2 \cdot \left(\sqrt{\sigma_g} + 1\right)^2}. \tag{25}$$

Summarizing the conclusions discussed in this section, we will draw certain conclusions:

- Having considered the properties of the skin effect, it is obvious that for existing photocells with a conductivity of hundreds of S/m (less often thousands), it can be argued that the main power of the electromagnetic wave will propagate both over the surface of the cell and throughout its entire body.
- Based on the first statement, when 3D simulating a photocell, it is necessary to perform "solve inside".
- Since we use empirical expressions that provide calculated accuracy no worse than 2–3%, we can assume that the accuracy of estimating the electrical characteristics of the photocells under study will be within these limits (without taking into account measurement errors).

Consequently, the mentioned expressions may be used to ascertain the basic characteristics of photocells based on the measured complex transmission coefficients when they are mounted in the experimental setup.

4. EXPERIMENTAL RESULTS

We have developed the experimental setup measuring S-parameter; VNA C2409 4-Port [44] was used as the measuring instrument. This VNA enables measurement of S-parameters in a frequency range from 100 kHz to 9 GHz. We calibrated the VNA with the coaxial cable to eliminate their influence on the measurement result in the frequency range from 1 MHz to 9 GHz.

We selected a 450 nm laser [45] with a maximum output power of 400 mW for the experimental setup. The choice of the laser is due to the following factors:

- convenience of aiming the laser at the photosensitive area in the visible range of the spectrum (the laser illuminated the installed photocell, completely covering the photosensitive area without going beyond it);
- discrete radiation power control with a step of 1% of its maximum radiation power (the laser radiation power was controlled with a digital controller);
- ability to adjust the laser spot with the built-in optical system;
- significant maximum radiation power (which is rarely observed in similar laser setups).

We selected the distance between the laser and a photocell to be 0.8 m. The distance was selected to adjust the laser spot more convenient, and it is safe for illuminating photocells at this distance without damaging them. The laser was calibrated at the same distance.

Figure 11 shows a circuit board with a GCPW, 50 Ohm impedance, in the gap of which studied photocells can be installed. This circuit board is made of Rogers RO4003 material. The circuit board has SMA (Female) connectors on both sides. The SMA connectors are connected to the VNA with coaxial

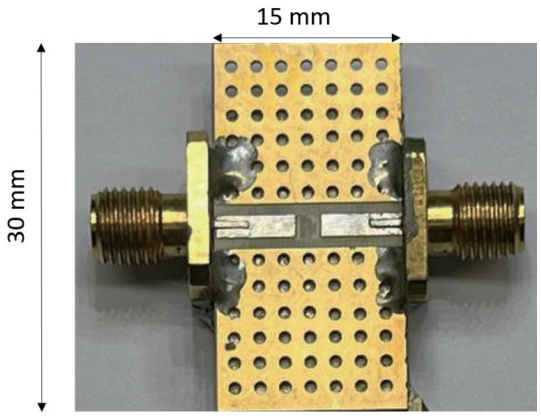

FIGURE 11. The experimental setup for measurements of photocell parameters.

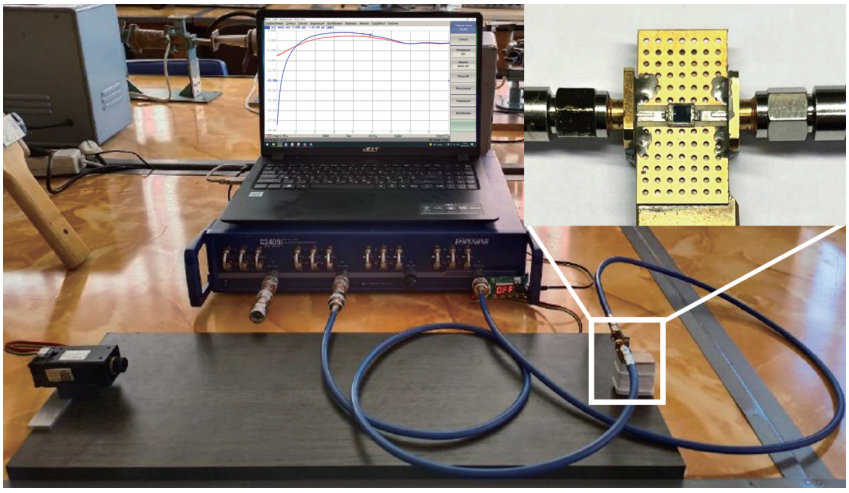

FIGURE 12. The process of measuring the characteristics of a photocell at different luminous flux power values.

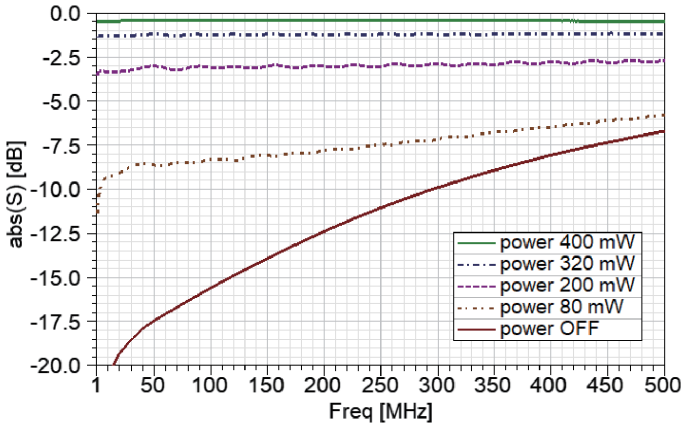

FIGURE 13. The measured $|S_{21}|$ plots with the SFH203P photodiode under study.

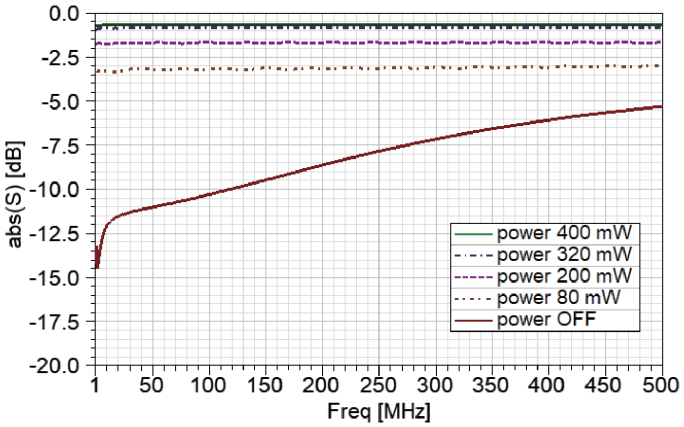

FIGURE 14. The measured $|S_{21}|$ plots with the VBW34 photodiode under study.

cables (Figure 12). Such a circuit allows us to measure the S-parameters of a photocell as a part of the transmission line with 50 Ohm impedance. We performed all the measurements on the described experimental setup in a dark room isolating the studied photocell from external light sources.

We have measured three photodiode samples: SFH203P, VBW34, and VBPW34S; three photoresistor GL55 samples with resistance values of 0.5 MOhm, 2 MOhm, and 4 MOhms; and four phototransistor samples: BPW85C, L-7113P2C, TEPT4400, and KP-3216P3C.

4.1. Photodiodes Measurements

Figures 13–15 show the absolute transmission coefficients ($|S_{21}|$) measured at frequencies from 1 to 500 MHz at different laser power levels with a photodiode installed on the setup.

The measurement results indicate that the photodiode in the experimental setup does not conduct without illumination, and the attenuation in the transmission line ranges from 10 to 20 dB in the lower frequency range of the experiments performed. As the laser power increases, the line loss decreases, and as we can see at the maximum radiation power of 400 mW, the modulus of the transmission coefficient is less than 1 dB over the entire measured frequency range.

It should be noted that the transmission coefficient absolutes increase with the measured frequency. At 500 MHz and higher, it is obvious that the cell transmits the most power even without light. This can be explained because of the photodiode's capacitive properties (Figure 2), which become more expressed as the frequency increases.

4.2. Photoresistors Measurements

Figures 16–18 show the absolute transmission coefficients ($|S_{21}|$), measured at frequencies from 1 to 500 MHz at different laser power levels with a photoresistor installed on the experimental setup.

Plots of the photoresistor data show that the transmission coefficients' frequency dependences perform closely to the photodiode manner. In the tested frequency range, it is impossible to achieve a line loss value of less than 5 dB while operating with resistors, even at the maximum light intensity. Moreover, the value of losses in the line with an installed photoresistor varies depending on the nominal resistance of the photocell. For ex-

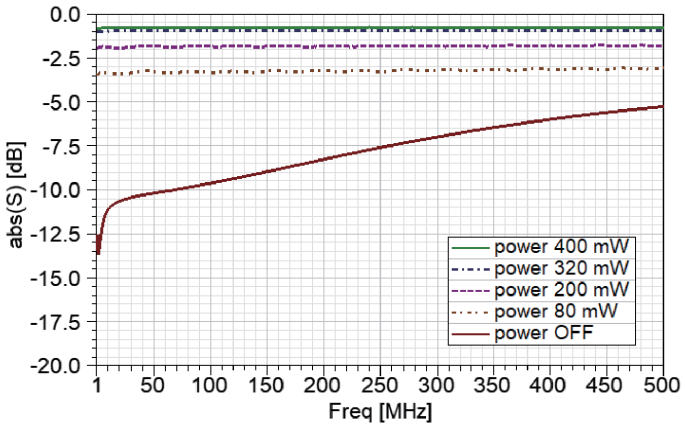

FIGURE 15. The measured $|S_{21}|$ plots with the VBPW34S photodiode under study.

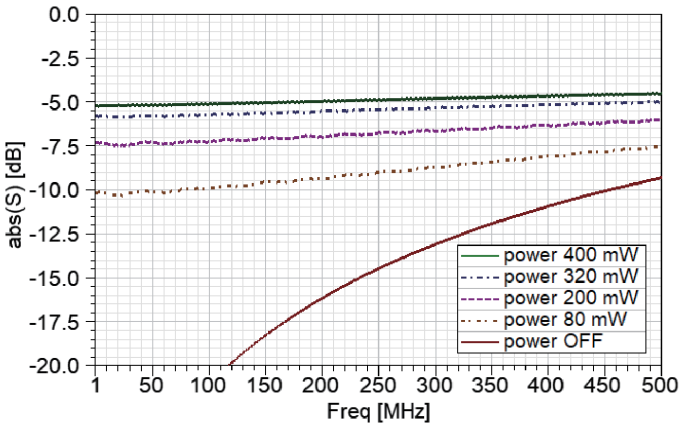

FIGURE 16. The measured $|S_{21}|$ plots with the GL55 photoresistor (0.5 MOhm) under study.

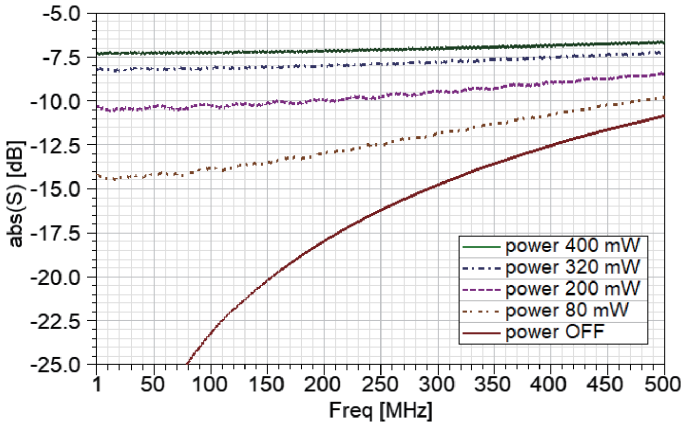

FIGURE 17. The measured $|S_{21}|$ plots with the GL55 photoresistor (2.0 MOhm) under study.

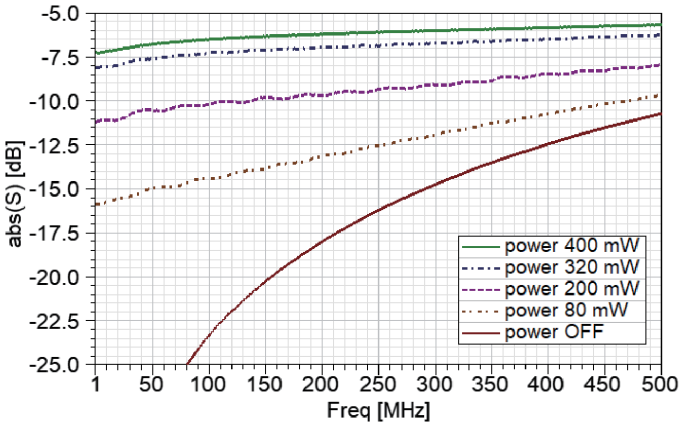

FIGURE 18. The measured $|S_{21}|$ plots with the GL55 photoresistor (4.0 MOhm) under study.

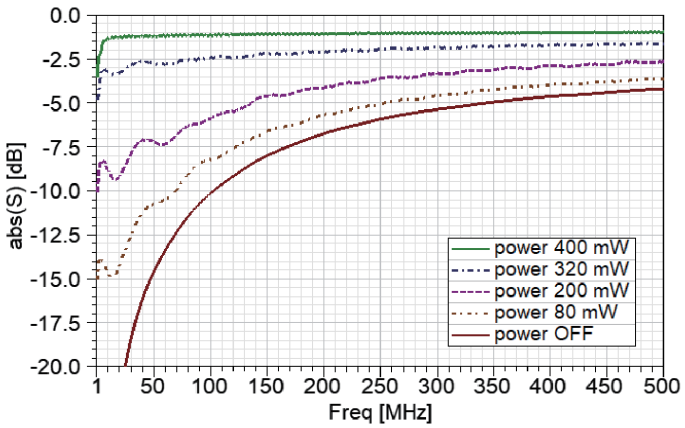

FIGURE 19. The measured $|S_{21}|$ plots with the BPW85C phototransistor under study.

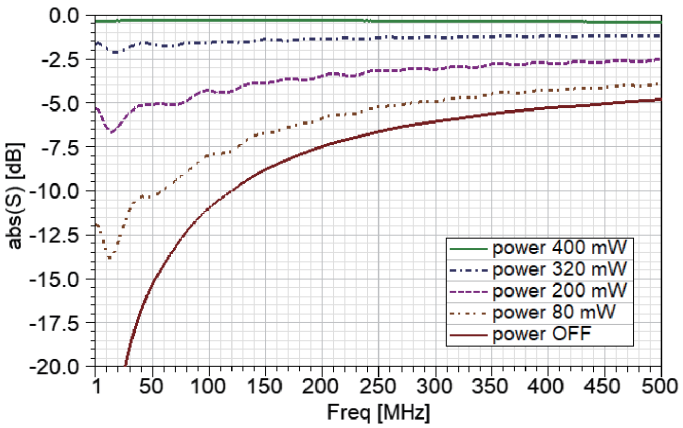

FIGURE 20. The measured $|S_{21}|$ plots with the L-7113P2C phototransistor under study.

ample, for the photoresistor with a nominal resistance value of 0.5 MOhm, the $|S_{21}|$ value at the maximum power of the illumination was -5 dB; for the photoresistor with a nominal resistance value of 2.0 MOhm, at the maximum laser power, the $|S_{21}|$ value was about -7.5 dB. Similar to photodiodes, photoresistors have capacitive properties (Figure 4), which become more and more apparent as the frequency of the RF signal passing through the measurement setup increases.

4.3. Phototransistors Measurements

Figures 19–22 show absolute transmission coefficients ($|S_{21}|$), measured at frequencies from 1 to 500 MHz at different laser

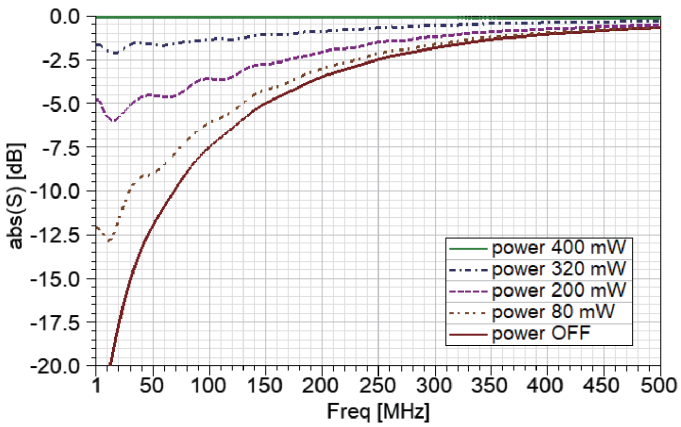

FIGURE 21. The measured $|S_{21}|$ plots with the TEPT4400 phototransistor under study.

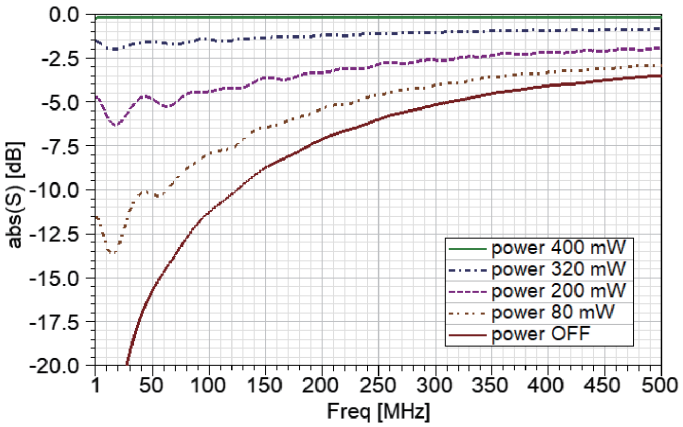

FIGURE 22. The measured $|S_{21}|$ plots with the KP-3216P3C phototransistor under study.

power levels with a phototransistor installed on the experimental setup.

From the results obtained during the measurements of phototransistors, we see that the curves and their behavior in the frequency domain are similar to the behavior of the curves obtained during the studies of photodiodes. However, at the maximum power of the laser for most of the photocells (except BPW85C), we see a significant increase in the transmission coefficients absolutes (which means a significant decrease in losses due to the increase in the conductivity of the studied photocell).

Like the previously studied photocells, phototransistors have capacitive properties (Figure 5), which leads to a decrease in the resistance of the cell with increasing frequency of the radio frequency signal passing through it (regardless of the presence of light and its power). However, as we see, these properties for different cells show differently; for example, for TEPT4400 photocell, the value of the transmission coefficients absolutes at 500 MHz is indistinguishable for different laser power levels, while for L-7113P2C photocell, the difference between the transmission coefficients absolutes at the lowest and highest laser power levels is more than 5 dB, and such a photocell at 500 MHz still has the properties of an optical semiconductor.

4.4. Analysis of Measured Results

To calculate the conductivity of a photocell by the suggested formula (25), the cell is placed on the substrate (Figures 9 and 12), and impedance is estimated taking into account the geometrical dimensions of the photocell and ε_{PC} value according to the expressions (20) and (1)–(3). To estimate the "$-L_{SMA}$" multiplier value from expression (25), the connector loss value is taken from the appropriate technical documentation; to estimate the "$-L_{TRL}$" loss value, calculations are performed using formulas (4)–(8). A simpler and more accurate technique to estimate "$-L_{SMA}$" and "$-L_{TRL}$" multipliers values is to measure the line loss before making a place to install a photocell. Likewise, according to expression (20), the phase incursion when the signal passes through the microstrip line where the photocell being studied is installed is determined as the difference between the arguments of the transmission coefficient (S_{21}) measured on the experimental setup with the optical element in place and that measured on the setup before cutting the slot at the center for its installation.

At first, we must determine the relative permittivity (20) of studied photocells at different power levels of the laser used (including the light flux absence when a laser is turned off). Second, we determine the impedances of the photocells (1)–(3), presented as a small segments of a transmission line based on calculated effective permittivity (19). Next, we estimate the conductivities of the calls using formula (25).

One photocell from each group was selected for the estimation of conductivity; they are GL55 photoresistor with a nominal of 0.5 MOhm, SFH203P photodiode, and KP-3216P3C phototransistor. Figures 23–25 show the frequency dependences of the transmission coefficients arguments in the study of the GL55 photoresistor rated 0.5 MOhm, the SFH203P photodiode, and the KP-3216P3C phototransistor, respectively. The relative permittivity of the cells was calculated using formula (20); the results are shown in Figures 26–28.

From the results obtained (Figures 26–28), we see quite high permittivity values, which suggests that the impedances for different photocells will be very different at different laser power levels. That is, we cannot neglect this fact and accept, for example, $Z_{PC} = 50$ Ohm. It is more convenient to use expressions (1)–(3) to calculate the required width w of an MTL stripline. To calculate the impedance, it is more convenient to use the formulas given in [41–43], for example:

for $w/h \leq 1$:

$$Z = \frac{60}{\sqrt{\varepsilon_{re}}} \cdot \ln\left(\frac{8h}{w} + 0.25\frac{w}{h}\right), \tag{26}$$

for $w/h \geq 1$:

$$Z = \frac{120\pi}{\sqrt{\varepsilon_{re}}} \cdot \left[\frac{w}{h} + 1.393 + 0.677\ln\left(\frac{w}{h} + 1.444\right)\right]^{-1}; \tag{27}$$

and for a GCPW:

$$Z = \frac{30\pi}{\sqrt{\varepsilon_{re}}} \cdot \left[\frac{K'(k_1)}{K(k_1)}\right]. \tag{28}$$

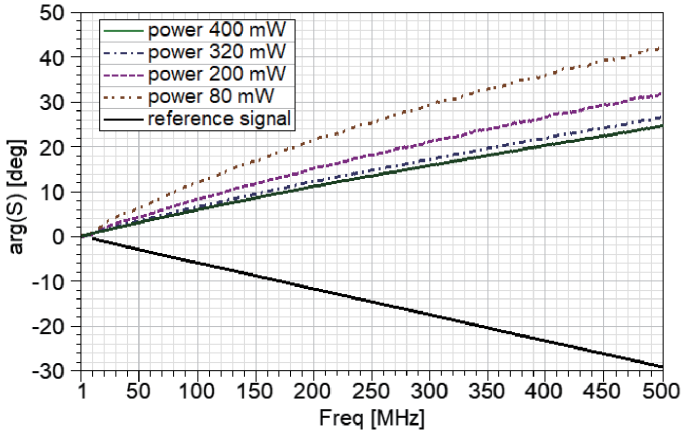

FIGURE 23. The measured arg(S_{21}) plots with the GL55 photoresistor (0.5 MOhm) under study.

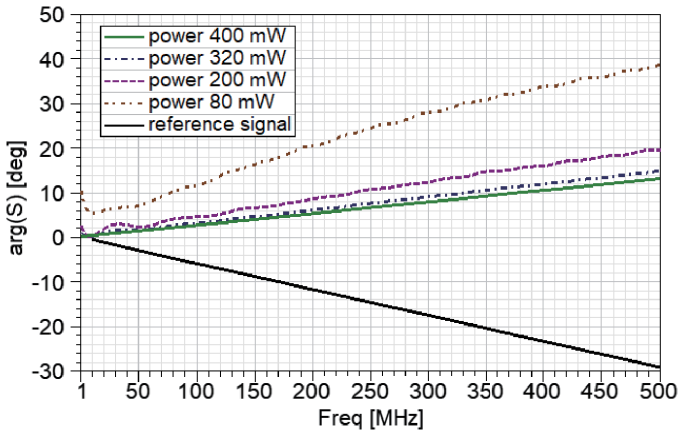

FIGURE 24. The measured arg(S_{21}) plots with the SFH203P photodiode under study.

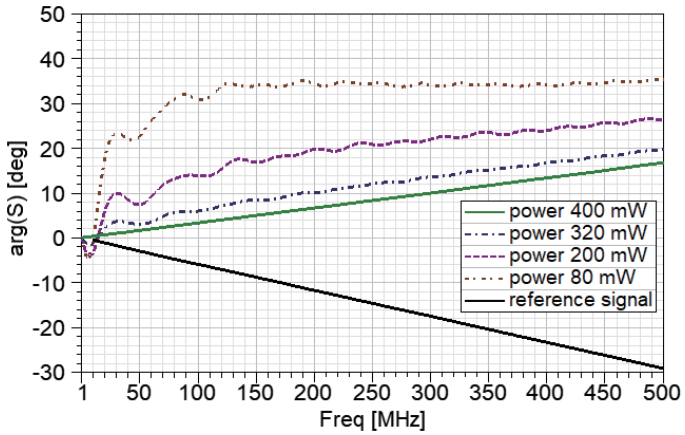

FIGURE 25. The measured arg(S_{21}) plots with the KP-3216P3C phototransistor under study.

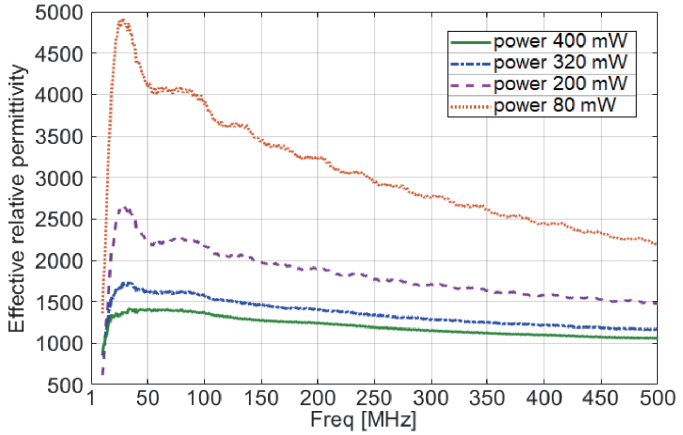

FIGURE 26. The permittivity plots obtained with the measured arg(S_{21}) with the GL55 photoresistor (0.5 MOhm) under study.

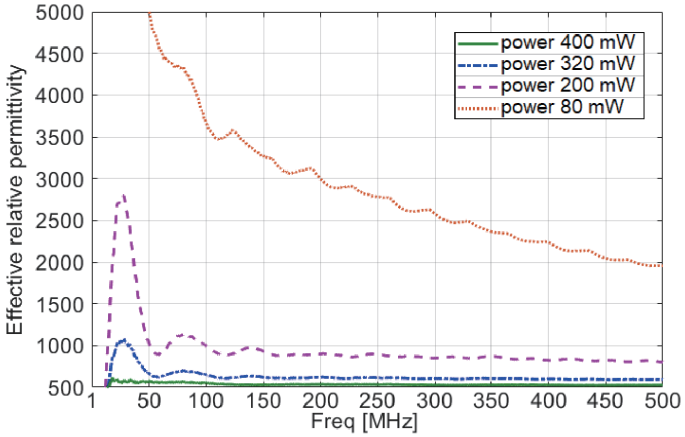

FIGURE 27. The permittivity plots obtained with the measured arg(S_{21}) with the SFH203P photodiode under study.

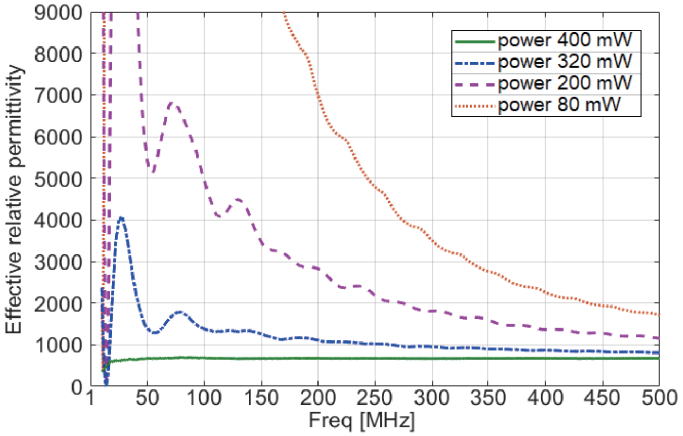

FIGURE 28. The permittivity plots obtained with the measured arg(S_{21}) with the KP-3216P3C phototransistor under study.

Figure 29 shows the conductivity plots of the GL55 photoresistor of 0.5 MOhm resistance nominal, calculated based on the measured transmission coefficients on the experimental setup. Obviously, such photoresistors cannot be used as keys in the design of microwave devices or antennas since, even at maximum laser power, the cell conductivity is only several dozens of S/m, resulting in line losses of several decibels with the installed photocell. However, such cells can be used where re-

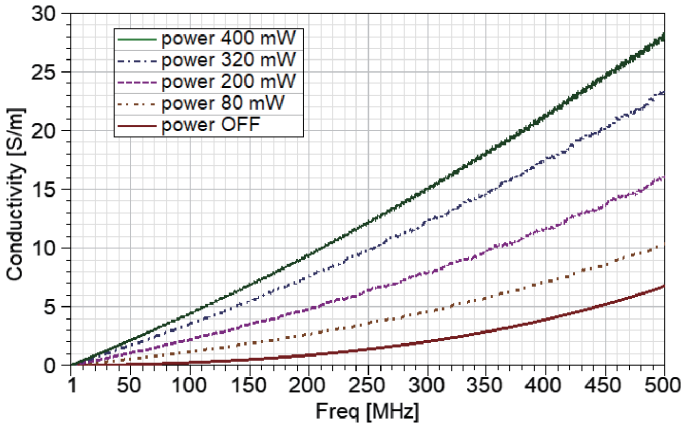

FIGURE 29. The conductivity plots obtained with the measured S_{21} with the GL55 photoresistor (0.5 MOhm) under study.

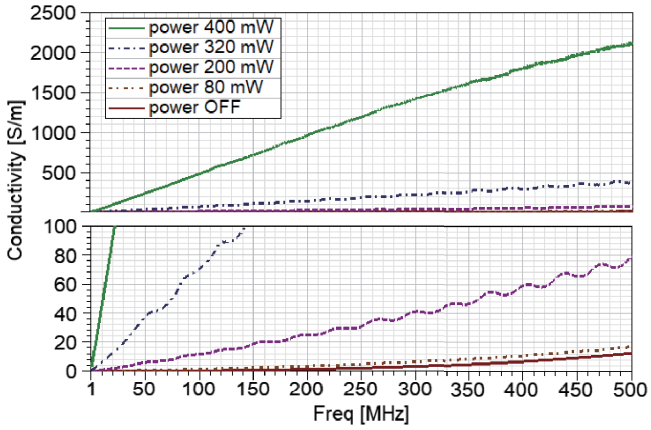

FIGURE 30. The conductivity plots obtained with the measured S_{21} with the SFH203P photodiode under study.

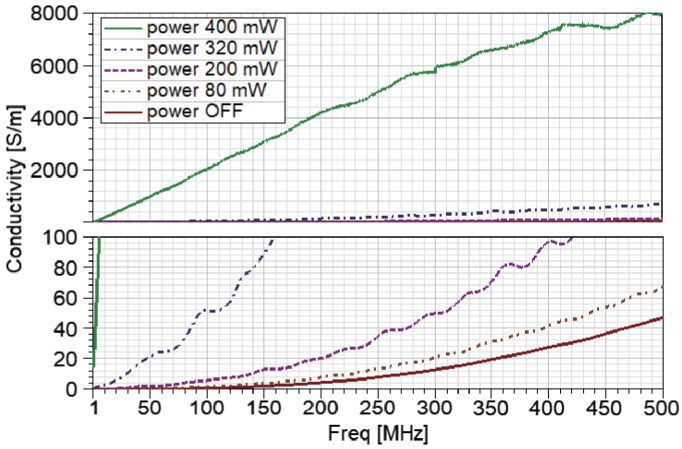

FIGURE 31. The conductivity plots obtained with the measured S_{21} with the KP-3216P3C phototransistor under study.

sistance changes are required in the operation of the product, such as tuning attenuators, various power dividers, and directional couplers. The values of conductivity obtained based on the proposed method can be used in simulating such devices during their design, and controlling the photocell by an optical line will significantly improve the characteristics of the final product.

Figures 30 and 31 show the frequency dependences of the conductivities of the SFH203P photodiode and KP-3216P3C phototransistor calculated under the measured transmission coefficients on the experimental setup at different levels of laser radiation power. As can be seen from the plots, at the maximum power of the laser, the photocells have a very significant level of conductivity, which reaches 2000 S/m for the example of photodiode and 8000 S/m for the example of phototransistor at the upper edge of the studied frequency range -500 MHz. Such characteristics will allow the use of such photocells as keys in microwave circuits, for example, in developing a phase shifter, an antenna with switchable characteristics (frequency range, type, or direction of rotation polarization, etc.) In addition, the high conductivity value of the photoresistor will allow such a photocell to be used in antenna or microwave technology as part of a radiating system, i.e., as a radiating conductor.

Consequently, we used the example of three photocells to identify the main electrical characteristics at various power levels of light flux directed onto the photosensitive surface.

While understanding a photocell as a section of a transmission line, we can talk about reflections (or S_{11} values) due to the significant change in a relative permittivity (an effective relative permittivity) and the associated change in impedance. In a similar way, by measuring the absolutes and arguments of the reflection coefficient, it is possible to determine the dielectric constant of the element for use in the future in 3D simulation. However, we believe that the transmission coefficient method is the most convenient and understandable and allows us to evaluate both the conductivity and permittivity of the photocell under study.

5. PHOTOCELL PARAMETERS CALCULATION RESULTS APPLICATION IN SIMULATION

To evaluate the obtained calculated values of conductivities and dielectric constants of the photocells, we performed a simula-

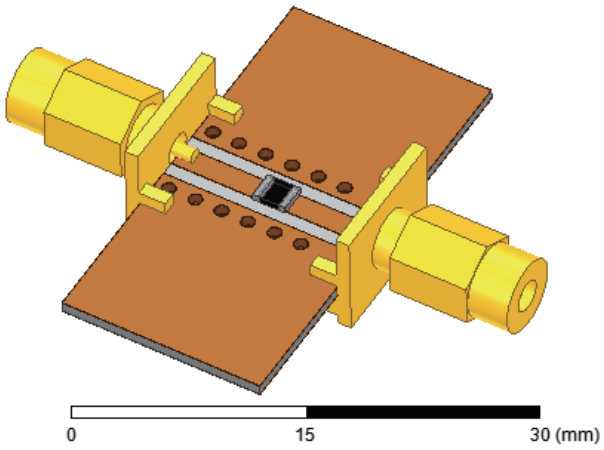

FIGURE 32. The experimental setup model in HFSS Design.

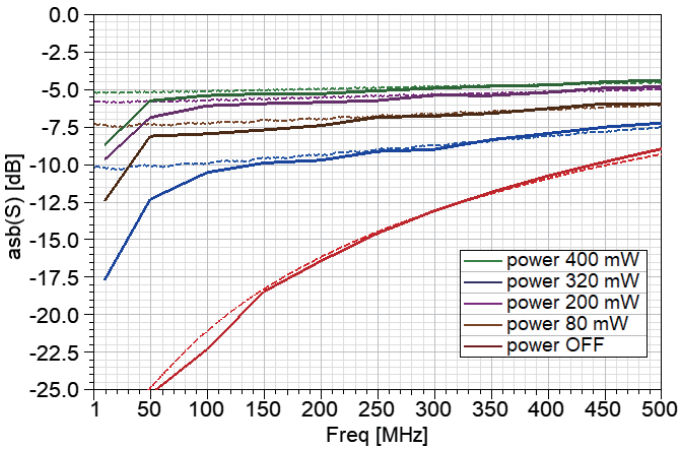

FIGURE 33. The S-parameters plots with the GL55 photoresistor (0.5 MOhm) under study (solid — simulated, dash — measured).

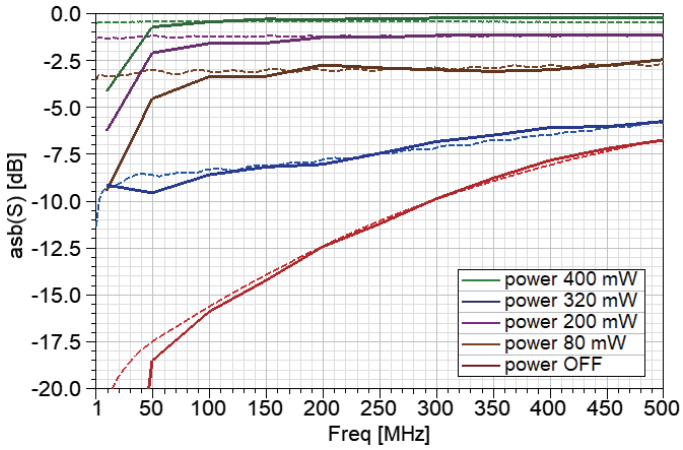

FIGURE 34. The S-parameters plots with the SFH203P photodiode under study (solid — simulated, dash — measured).

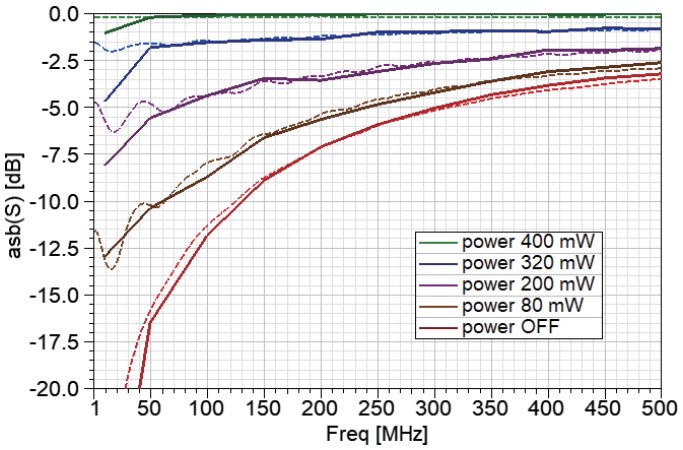

FIGURE 35. The S-parameters plots with the KP-3216P3C phototransistor under study (solid — simulated, dash — measured).

tion based on a transmission line, as shown in Figure 7. The dielectric with parameters ($\varepsilon = 3.55$, tg$\delta = 0.0027$), matching the RO4003 material, was set as the substrate; the line width is chosen according to the wave impedance of 50 Ohm; SMA connectors (50 Ohm) are modeled at the edges of the PCB. The simulation is performed in the HFSS Design software module of the ANSYS EM Suite. We chose the previously studied photocells as examples: photoresistor GL55 with a resistance nominal value of 0.5 MOhm, photodiode SFH203P, and phototransistor KP-3216P3C.

In the center of the experimental setup model, a 2 mm gap in the transmission line was made (similar to what was done in the experiment). A rectangle-shaped photocell model, as shown in Figure 32 with calculated material characteristics, is placed on the gap. On the edges of the rectangle (photocell), models of metal parts responsible for communication with the transmission line are made. For the photocell model, frequency dependencies are set based on the calculated values of conductivity and dielectric constant. We took the size of the photocell in the model according to its actual dimensions taken from the corresponding datasheet.

Figures 33–35 show the transmission coefficient plots that we obtained through simulation. From the presented results, we see the similarity of the values of the transmission coefficients absolutes in the line obtained by simulation with the measured values. As can be seen, there is a discrepancy in the lower part of the frequency range in some plots (Figures 33 and 34). The following is associated with the semiconductor's measurement technique, measurement device, and simulation peculiarities that are inappropriate for certain physical processes. As frequency and conductivity increase, high similarity in the behavior of curves is observed in all plots.

Therefore, the methodology proposed in the article allows us to determine with some accuracy the characteristics of the applied optical cells and further use these values in simulating antennas and microwave devices based on photocells with variable conductivity, including the development of plasma antennas.

6. CONCLUSION

Purchased photocells, such as photoresistors, photodiodes, and phototransistors, have been studied in this article. The studied elements change their conductive properties under light of different powers, which should be considered during microwave devices (or antennas) simulation where the semiconductor is supposed to be used. We obtained measured absolute transmission coefficients and argument plots for each cell with a transmission line in the gap.

In 3D simulation, basic characteristics such as conductivity, relative permeability or relative permittivity, and dielectric loss tangent, are specified for a bulk or planar element. Photocells do not have magnetic properties; in this regard, the conductivity (including the values of the loss tangent) and relative permittivity remain important for them. To determine the values of these characteristics, we propose a method based on the measurement of complex transmission coefficients using a simple transmission line.

The method is based on the representation of the photocell as a small segment of a transmission line, for which the values of conductivity and permittivity are determined under the measured complex transmission coefficients at different power levels of the light illumination acting on the photocell and at different frequencies. The obtained values are set for the element in three-dimensional simulation, which is most often used in antenna design.

The simulation results and transmission coefficient measurements indicate that the curves are similar, meaning that the technique covered in the article can be used to find the necessary semiconductor settings for simulation.

During the research, we also obtained the results of measurements of some photocells, among which were three samples of photodiodes: SFH203P, VBW34, and VBPW34S; three samples of GL55 photoresistors with resistance values of 0.5 MOhm, 2 MOhm, and 4 MOhm; and four samples of phototransistors: BPW85C, L-7113P2C, TEPT4400, and KP-3216P3C. The analysis of the measured plots shows that the considered cells are increasingly dominated by conductor properties with increasing frequency, which is related to their capacitive characteristics (shown in Section 2 of this article). In the studied frequency range, from the point of view of the transition from the dielectric to the conductor state, the best results were shown by phototransistors.

The results in this article are undoubtedly important for researchers and developers studying plasma antennas or antennas with switchable parameters based on the use of semiconductor cells (including optical ones). This subject is relevant and requires further in-depth study.

REFERENCES

[1] Cohen, R. S., L. S. Jr., and P. M. Routly, "The electrical conductivity of an ionized gas," *Physical Review*, Vol. 80, No. 2, 230, 1950.

[2] Lin, S.-C., E. L. Resler, and A. Kantrowitz, "Electrical conductivity of highly ionized argon produced by shock waves," *Journal of Applied Physics*, Vol. 26, No. 1, 95–109, 1955.

[3] Lamb, L. and S.-C. Lin, "Electrical conductivity of thermally ionized air produced in a shock tube," *Journal of Applied Physics*, Vol. 28, No. 7, 754–759, 1957.

[4] Anderson, T., *Plasma Antennas. Second Edition*, Artech House, 2021.

[5] Kumar, V., M. Mishra, and N. K. Joshi, "Study of a fluorescent tube as plasma antenna," *Progress In Electromagnetics Research Letters*, Vol. 24, 17–26, 2011.

[6] Magarotto, M., F. Sadeghikia, L. Schenato, D. Rocco, M. Santagiustina, A. Galtarossa, A. K. Horestani, and A.-D. Capobianco, "Plasma antennas: A comprehensive review," *IEEE Access*, Vol. 12, 80 468–80 490, 2024.

[7] Wang, L., P. Sun, Y. You, A. Mikul, R. Bonebright, G. A. Kromholtz, and D. Heo, "Highly linear Ku-band SiGe PIN diode phase shifter in standard SiGe BiCMOS process," *IEEE Microwave and Wireless Components Letters*, Vol. 20, No. 1, 37–39, 2009.

[8] De Luis, J. R. and F. de Flaviis, "A reconfigurable dual frequency switched beam antenna array and phase shifter using PIN diodes," in *2009 IEEE Antennas and Propagation Society International Symposium*, 1–4, North Charleston, SC, USA, Jul. 2009.

[9] Trinh, K. T., J. Feng, S. H. Shehab, and N. C. Karmakar, "1.4 GHz low-cost PIN diode phase shifter for L-band radiometer antenna," *IEEE Access*, Vol. 7, 95 274–95 284, 2019.

[10] Shishkin, M. and S. Shabunin, "Analysis of influence of the clustering degree of the antenna array on its radiation characteristics," in *AIP Conference Proceedings*, Vol. 2466, No. 1, 2022.

[11] Hindle, P., "The state of RF/microwave switches," *Microwave Journal*, Vol. 53, No. 11, 20–36, 2010.

[12] Deng, P.-H., J.-T. Tsai, and R.-C. Liu, "Design of a switchable microstrip dual-band lowpass-bandpass filter," *IEEE Microwave and Wireless Components Letters*, Vol. 24, No. 9, 599–601, 2014.

[13] Ghorbani, F., A. Dayan, J. Zhou, Y. Huang, A. G. Schuchinsky, and M. Gustafsson, "Linearity enhancement in PIN-diode-based switches," *IEEE Transactions on Microwave Theory and Techniques*, 1–12, 2024.

[14] Jung, D., T. Fukusako, N. Kitamura, N. Mita, and C. Ha, "Polarization switchable microstrip antenna using PIN diodes," *IEICE Transactions on Communications*, Vol. 87, No. 1, 152–157, 2004.

[15] Ushijima, Y., E. Nishiyama, and M. Aikawa, "Single layer extensible microstrip array antenna integrating SPDT switch circuit for linear polarization switching," *IEEE Transactions on Antennas and Propagation*, Vol. 60, No. 11, 5447–5450, 2012.

[16] Chitra, R. J. and V. Nagarajan, "Frequency reconfigurable antenna using PIN diodes," in *2014 Twentieth National Conference on Communications (NCC)*, 1–4, Kanpur, India, May 2014.

[17] Bhattacharya, A. and R. Jyoti, "Frequency reconfigurable patch antenna using PIN diode at X-band," in *2015 IEEE 2nd International Conference on Recent Trends in Information Systems (ReTIS)*, 81–86, Kolkata, India, Jul. 2015.

[18] Boufrioua, A., "Frequency reconfigurable antenna designs using PIN diode for wireless communication applications," *Wireless Personal Communications*, Vol. 110, No. 4, 1879–1885, 2020.

[19] Rathore, P. S., R. Mali, R. Jatav, and M. K. Meshram, "A multifunctional antenna with high isolation for interweave and underlay operation in cognitive radio," *Progress In Electromagnetics Research B*, Vol. 108, 105–119, 2024.

[20] Agarwal, S., A. Singh, and M. K. Meshram, "A low-profile single-layered wideband combinational reconfigurable antenna for 4G and 5G applications," *Progress In Electromagnetics Research B*, Vol. 109, 17–28, 2024.

[21] Su, H., H. Hu, H. Zhang, B. Wang, H. Kang, Y. Wang, and M. Hao, "Investigation of surface PiN diodes for a novel reconfigurable antenna," *Solid-State Electronics*, Vol. 139, 48–53, 2018.

[22] Kim, D.-J., E.-S. Jo, Y.-K. Cho, J. Hur, C.-K. Kim, C. H. Kim, B. Park, D. Kim, and Y.-K. Choi, "A frequency reconfigurable dipole antenna with solid-state plasma in silicon," *Scientific Reports*, Vol. 8, No. 1, 14996, 2018.

[23] Hur, J., I.-J. Nam, Y.-K. Cho, D.-J. Kim, E.-S. Jo, S. Lee, C.-K. Kim, G.-B. Lee, C. H. Kim, S. B. Hyun, D. Kim, and Y.-K. Choi, "Reconfigurable beamforming silicon plasma antenna with vertical PIN diode array," *Advanced Electronic Materials*, Vol. 6, No. 12, 2000257, 2020.

[24] Pascaud, R., F. Pizarro, O. Pascal, T. Callegari, and L. Liard, "Theoretical and numerical study of a plasma-based frequency tunable microstrip antenna," in *The 8th European Conference on Antennas and Propagation (EuCAP 2014)*, The Hague, Netherlands, Apr. 2014.

[25] Kang, H. Y., H. Y. Hu, B. G. Han, and H. Su, "A reconfigurable solid-state plasma dipole antenna based on SPiN diodes," *Microelectronic Engineering*, Vol. 214, 55–59, 2019.

[26] Ojaroudi Parchin, N., H. J. Basherlou, Y. I. A. Al-Yasir, A. M. Abdulkhaleq, and R. A. Abd-Alhameed, "Reconfigurable antennas: Switching techniques — A survey," *Electronics*, Vol. 9, No. 2, 336, 2020.

[27] Mora-Seró, I., G. Garcia-Belmonte, P. P. Boix, M. A. Vázquez, and J. Bisquert, "Impedance spectroscopy characterisation of highly efficient silicon solar cells under different light illumination intensities," *Energy & Environmental Science*, Vol. 2, No. 6, 678–686, 2009.

[28] Khan, F., S. N. Singh, and M. Husain, "Effect of illumination intensity on cell parameters of a silicon solar cell," *Solar Energy Materials and Solar Cells*, Vol. 94, No. 9, 1473–1476, 2010.

[29] Yon, H., A. H. Awang, M. T. Ali, S. Subahir, S. N. Kamaruddin, M. A. Aris, and N. A. Wahab, "Integrated stacked microstrip antenna with Light Emitting Diode (LED) for Wi-Fi application," *Journal of Telecommunication, Electronic and Computer Engineering (JTEC)*, Vol. 8, No. 6, 83–86, 2016.

[30] Patron, D., A. S. Daryoush, and K. R. Dandekar, "Optical control of reconfigurable antennas and application to a novel pattern-reconfigurable planar design," *Journal of Lightwave Technology*, Vol. 32, No. 20, 3394–3402, 2014.

[31] Panagamuwa, C. J., A. Chauraya, and J. C. Vardaxoglou, "Frequency and beam reconfigurable antenna using photoconducting switches," *IEEE Transactions on Antennas and Propagation*, Vol. 54, No. 2, 449–454, 2006.

[32] Ramos-Hernanz, J. A., J. J. Campayo, E. Zulueta, O. Barambones, *et al.*, "Obtaining the characteristics curves of a photocell by different methods," in *International Conference on Renewable Energies and Power Quality*, Vol. 11, 1–6, 2013.

[33] Tada, K., "Parameter extraction from S-shaped current-voltage characteristics in organic photocell with opposed two-diode model: Effects of ideality factors and series resistance," *Physica Status Solidi (A)*, Vol. 212, No. 8, 1731–1734, 2015.

[34] Muller, M. F., *Photovoltaic Modeling Handbook*, John Wiley & Sons, 2018.

[35] García, Y. and F. G. Reina, "Mathematical model for the determination of volt-ampere characteristics in solar photocells," *Revista Colombiana de Tecnologías de Avanzada*, Vol. 2, 105–111, 2022.

[36] Dobrev, G., N. Paunkov, R. Terzieva, M. Matsankov, I. Naydenova, and D. Budakova, "Algorithm for determining photoresist characteristics," in *Environment. Technology. Resources. Proceedings of the 15th International Scientific and Practical Conference*, Vol. 2, 364–370, 2024.

[37] Gevorgian, S. S., "Design considerations for an optically excited semiconductor microstrip gap at microwave frequencies," *IEE Proceedings, Part J — Optoelectronics*, Vol. 139, No. 2, 153–157, 1992.

[38] Ross, D. A., *Optoelectronic Devices and Optical Imaging Techniques*, Red Globe Press London, 1979.

[39] Zhang, H., X. Zhang, C. Liu, S.-T. Lee, and J. Jie, "High-responsivity, high-detectivity, ultrafast topological insulator bi2se3/silicon heterostructure broadband photodetectors," *ACS Nano*, Vol. 10, No. 5, 5113–5122, 2016.

[40] Xie, H., J. Wu, D. Sun, S. Liu, R. Liu, W. Zhang, and X. Yi, "Modeling and analysis of an uni-traveling carrier herterojucntion phototransistor," in *2017 International Conference on Circuits, System and Simulation (ICCSS)*, 28–31, London, UK, Jul. 2017.

[41] Hong, J. S., *Microstrip Filters for RF/Microwave Applications*, John Wiley & Sons, 2011.

[42] Fusco, V. F., *Microwave Circuits: Analysis and Computer-Aided Design*, Prentice Hall, 1988.

[43] Bahl, I., *Microstrip Lines and Slotlines, Fourth Edition*, Artech House, 2024.

[44] C2409 4-Port 9 GHz Analyzer, https://coppermountaintech.com/vna/c2409-4-port-9-ghz-analyzer.

[45] NEJE N30610 450 nm laser module, https://neje.shop/products/7w-laser-module-7w-450nm-blu-ray-laser-engraving-machine-woodworking-machinery-parts-laser-deapth-diy-tools-for-master-series.